12-2021

Relationship Between Dike Injection and b-Value for Volcanic Earthquake Swarms

Allen F. Glazner
University of North Carolina

Stephen R. McNutt
University of South Florida, smcnutt@usf.edu

JGR Solid Earth

RESEARCH ARTICLE
10.1029/2020JB021631

Special Section:
Merging geophysical, petrochronologic and modeling perspectives to understand large silicic magma systems

Relationship Between Dike Injection and *b*-Value for Volcanic Earthquake Swarms

Allen F. Glazner[1] and Stephen R. McNutt[2]

[1]Department of Earth, Marine, and Environmental Sciences, University of North Carolina, Chapel Hill, NC, USA, [2]School of Geosciences, University of South Florida, Tampa, FL, USA

Abstract Dike swarms are the fossil remains of regions of the crust that have undergone repeated magma injections. Volcanic earthquake swarms and geodetic measurements are, at least in part, a record of active injection of fluids (water, gas, or magma) into fractures. Here, we link these two ways of observing magmatic systems by noting that dike thicknesses and earthquake magnitudes share similar scaling parameters. In the Jurassic Independence dike swarm of eastern California median dike thickness is ~1 m, similar to other swarms worldwide, but glacially polished exposures reveal that a typical dike comprises a number of dikelets that are lognormally distributed in thickness with a mean of ~0.1 m. Assuming that dikes fill penny-shaped cracks of a given aspect ratio, the geodetic moment and earthquake magnitude of a diking event can be estimated. A Monte Carlo simulation of dike-induced earthquakes based on observed dike thickness variations yields a frequency-magnitude distribution remarkably like observed volcanic earthquake swarms, with a *b*-value of ~1.7. We suggest that swarms of dikes composed of dikelets, as well as plutons built incrementally by sheet intrusions, are physical complements to volcanic seismic swarms, and that at least some earthquake swarms are a palpable expression of incremental magma emplacement.

Plain Language Summary Dike swarms are the geologically preserved expressions of magmatic intrusion. The dikes have different thicknesses, with many more small ones than large ones. We model the size distribution using Monte Carlo simulations and a variety of inputs. All yield similar numerical results with a value of the frequency-magnitude distribution of $b \sim 1.7$. This value is very close to observed seismic *b*-values for contemporary observations of earthquakes at active volcanoes. There are many more small earthquakes than larger ones, similar to the dike distributions. We suggest that the similar size distributions indicate that seismic swarms are the geophysical expression of the same processes that occur in dike formation.

Key Points:

- Dike swarms and volcanic earthquake swarms are different manifestations of similar phenomena
- They share similar scaling parameters
- A model linking dike injection to earthquake triggering yields a magnitude-frequency curve appropriate for volcanic earthquake swarms

Supporting Information:

Supporting Information may be found in the online version of this article.

Correspondence to:

A. F. Glazner,
afg@unc.edu

Citation:

Glazner, A. F., & McNutt, S. R. (2021). Relationship between dike injection and *b*-value for volcanic earthquake swarms. *Journal of Geophysical Research: Solid Earth*, *126*, e2020JB021631. https://doi.org/10.1029/2020JB021631

Received 29 DEC 2020
Accepted 4 NOV 2021

1. Introduction

1.1. Volcanic Earthquake Swarms and *b*-Value

Studies of volcanic plumbing systems are typically performed in two separate domains. Volcanic seismic swarms and geodetic measurements record unobservable movement of magma and other fluids in real time, whereas field exposures of dike swarms are observable, but inactive, records of past magma movement and emplacement. Here, we propose a simple physical model that links these two domains.

Active volcanic areas are typically host to swarms of small earthquakes that are related to movement of magma (e.g., Belachew et al., 2013; Benoit & McNutt, 1996; Farrell et al., 2010; Rubin et al., 1998; Ágústsdóttir et al., 2016), and may or may not result in an eruption. Long-period (LP; also called low frequency, LF) earthquakes and volcanic tremor are typically attributed to magma movement. In many instances at least some of the short-period (or high frequency, HF) earthquakes in a swarm exhibit non-double-couple focal mechanisms with a dilational component that is consistent with injection of magma or hydrothermal fluids (Julian, 1983; Miller et al., 1998; Saraò et al., 2001), but the proportion of such events is variable and generally small.

It is clear in many volcanic swarms that seismicity is triggered by magma movement even if the earthquakes are not directly a result of dilation. In a particularly well-studied example, Ágústsdóttir et al. (2016) showed that a 2-week earthquake swarm generated via propagation of a dike during the 2014 Bárðarbunga eruption in Iceland were predominantly strike-slip events with no volumetric components on steeply dipping faults near the dike tip. Nondouble-couple events with accompanying volume change were rare, and the total geodetic moment caused by dike intrusion was two orders of magnitude greater than the seismic moment release. It is likely that in general,

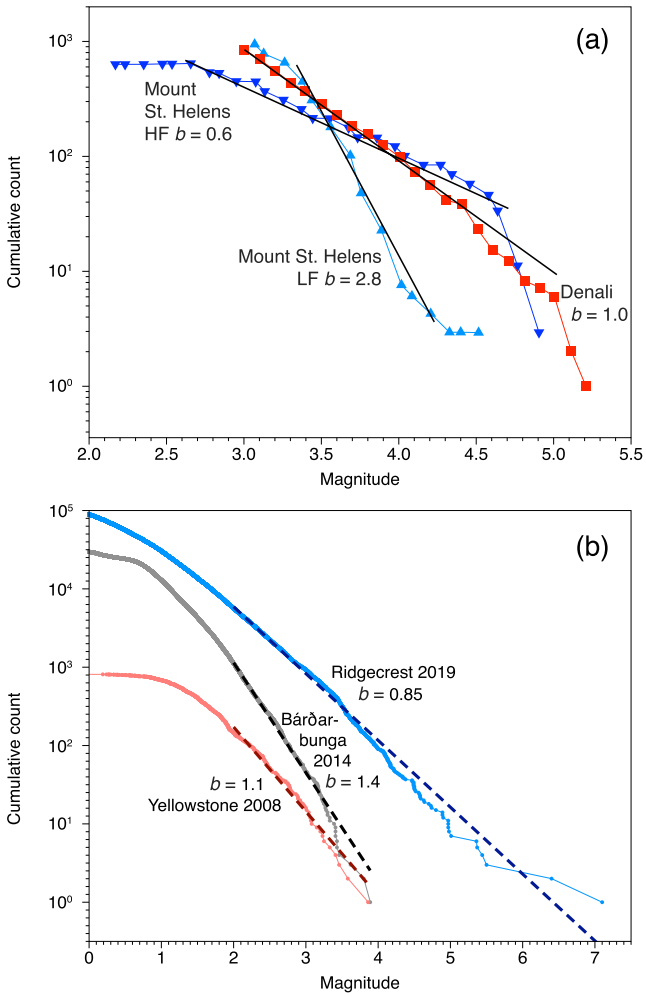

Figure 1. Representative *b*-value plots. (a) Representative plots for a tectonic earthquake sequence (aftershocks of the Denali earthquake, 2002) and volcanic swarms (Mount St. Helens 1980, divided into high-frequency and low-frequency events). These data, from Endo et al. (1981) and Ratchkovski et al. (2004), are plotted as cumulative numbers in magnitude bins. (b) Plots for the Ridgecrest 2019 tectonic earthquake sequence (Ross et al., 2019), Yellowstone 2008 volcanic earthquake swarm (Farrell et al., 2010), and the 2014 volcanic swarm at Bárðarbunga (Woods et al., 2018). Here, each event is plotted and the *b*-values are calculated by least squares fitting of all events with $M > 2.0$.

geodetic moment is greater than seismic moment, because it includes aseismic processes (references below in Section 6). For our purposes, the absolute values are less important. We are examining the distribution of the proportion of small versus large events, for both the earthquakes and the dikes.

Earthquake magnitude distributions are characterized by the parameter *b*, which is the negative of the slope on a plot of cumulative number of earthquakes *N* versus magnitude *M* (Gutenberg & Richter, 1954; Ishimoto & Iida, 1939, Figure 1):

$$log_{10}N = a - bM \quad (1)$$

where *N* is the cumulative number of earthquakes larger than magnitude *M* and *a* and *b* are constants.

These curves are anchored at the high *M* end by the largest earthquake in the catalog and are typically approximately linear down to an *M*-value where the curve flattens out. This is interpreted as the threshold of completeness or completeness magnitude (M_c) and the curve flattening represents the lower limit of sensitivity of the seismic array (Roberts et al., 2015). The *b*-value varies with physical parameters of a system, including state of stress (Scholz, 1968), pore pressure (Wyss, 1973), thermal gradient (Warren & Latham, 1970), and material heterogeneity (Mogi, 1963; see also Wiemer & McNutt, 1997 and references therein). Higher *b*-values mean a larger proportion of small earthquakes relative to large ones. Most plots using real data have a central part that is linear, and deviations at the two ends. The upper left end generally falls off below the M_c as described above, and the lower right end may be nonlinear due to sampling issues (too few events). Line fitting is generally done using weighted least squares or maximum likelihood algorithms (Aki, 1965; Bender, 1983; Utsu, 1965), which most closely fit the central linear portion of the data.

The *b*-values for sets of tectonic earthquakes are generally around 1.0, with a typical range of 0.8–1.2 (Figure 1, Frohlich & Davis, 1993). King (1983) and Huang and Turcotte (1988) explained values near unity as a natural consequence of the fractal nature of fault systems. In volcanic earthquake swarms, however, *b*-values are elevated, typically in the range 1.6–1.8 (Figure 1, McNutt, 2005; and Table A1). Further, *b*-values at volcanoes range from 0.5 to 2.1 for HF events to 1.4–3.7 for LF events (Table A1). Spatial mapping of *b*-values in volcanic areas reveals systematic variations with time and space that have been attributed to magma distribution; in particular, high *b*-values are associated with magma bodies (e.g., Wiemer et al., 1998; Wyss et al., 1997, Table A1).

Earthquake swarms at volcanoes have been extensively studied (McNutt & Roman, 2015, and references therein). In seismology, a swarm represents clustering in both time and space. A common definition is a "noticeable increase in seismicity rate above a visually established background seismicity rate without a clear triggering mainshock" (Holtkamp & Brudzinski, 2011). At volcanoes, durations range from hours to years with a geometric mean of 5.5 days, a median of 7 days, and a mode of 2 days for all swarms (sample: 385 swarms) using data from Benoit and McNutt (1996). If the swarms are divided into HF and LF events, the HF swarms last longer (geometric mean of 9.3 days; median 11 days; mode 8 days, sample: 104 swarms) and the LF swarms are relatively shorter (geometric mean of 5.5 days; median 5 days; mode 2 days, sample: 96 swarms). LF events are generally shallower than HF events, with depths of 1–3 km being representative for LF events and 3–12 km for HF events. Here we wish to compare the seismic *b*-values for contemporary earthquake swarms with the spatial geologic values for dike swarms from ancient intrusions. Thus, we need to establish which groups of seismic events offer the best basis for comparison.

1.2. Dike Swarms

Dike-sill complexes are increasingly recognized as the principal way in which magma moves in the upper crust (e.g., Coetzee & Kisters, 2016; Gudmundsson, 2020; Muirhead et al., 2014). Eroded volcanic areas commonly display steep radial or linear dike swarms that may be interconnected by sills (Galerne et al., 2011; Muirhead et al., 2016; Odé, 1957; Walker, 1986, 1999), and dike swarms hundreds to thousands of km long are common on the Earth and other planets (Ernst et al., 1995, 1997). Field data for this study were collected from the Late Jurassic Independence dike swarm (IDS) in California. Dikes in the IDS are exposed along a 600-km-long reach and were intruded parallel to the Late Jurassic belt of Jurassic plutons in the Sierra Nevada (Carl & Glazner, 2002). These dikes are overwhelmingly northwest-striking, steeply dipping, and andesitic to basaltic in composition (Glazner et al., 2008).

The commonly spectacular field exposures of dike swarms (Figure 2) make them ripe targets for statistical analysis. Dike thickness distributions generally have sharp lower cutoffs in the 1–10 cm range, medians around 50 cm, and a long right tail, yielding approximately lognormal distributions (Delaney & Gartner, 1997; Jolly & Sanderson, 1995; Walker et al., 1995; and below). For such distributions the geometric mean is a more accurate and less variable indicator of central tendency than the arithmetic mean. Dike thickness distributions are commonly described as power-law (Gudmundsson, 1995), but power-law distributions may be inappropriate because they do not honor the lower cutoff in thickness shown by field measurements (Jolly & Sanderson, 1995). Krumbholz et al. (2014) argued that the Weibull distribution makes a slightly better fit than the lognormal distribution and is better justified on mechanical grounds, but the lognormal distribution provides a good empirical fit and is mathematically simpler, so we have adopted it in this paper.

1.3. Linkages

Earthquakes and dike injection events both represent deformation, and both earthquake magnitudes and dike thicknesses have frequency distributions that decline exponentially with increasing size (i.e., lots of little ones and a few much larger ones). In this paper we present a hypothesis that links dike swarms to volcanic earthquake swarms via a simple mechanical model in which earthquakes are driven by stresses induced by dike injection. The model relies primarily on only one observational parameter, and using data from the Independence dike swarm gives a *b*-value in the range of those found for volcanic earthquake swarms.

1.4. Dike and Dikelet Thickness Distributions

Bartley et al. (2007) and Glazner et al. (2008) measured thicknesses of 705 dikes along a 200-km stretch of the IDS and found a lognormal distribution with a median width of 70 cm (Figure 3). Data used in this figure are tabulated in Table S1. In two areas of exquisite glacially polished exposure, they found that about half of the dikes are composite, composed of multiple injections (hereafter dikelets; Figure 2). Margins of dikelets are marked by chilled margins or sheets of wall rock ranging from slabs tens of cm thick to partially melted films only a few mm thick. Dikelets ($n = 287$) follow their own lognormal thickness distribution with a median of 9 cm (Figure 3, Glazner et al., 2008), and the average number of dikelets per dike was 3.1.

Measured dikelet thicknesses do not reflect the actual size distribution of magma injections because many dikelets split previous dikelets, producing half-dike pairs. For pure antitaxial injection, where each new dikelet intrudes the margin of the previous set, j injections will produce j dikelets. For pure syntaxial injection, where each new dikelet splits the previous one, j injections will produce $2j + 1$ dikelets. Benton et al. (2011) studied several thick, composite, glacially polished dikes in the Sierra Nevada. They compared dikelet compositions across dikes and commonly found mirror symmetry, a majority of dikes (33 of 56) with an odd number of dikelets (not counting those composed of a single pulse), and a dominance of syntaxial injection. Although the sample size is small, it is clear that at least some thick dikes were produced by syntaxial injection, as in Figure 2a, and thus the number of injections is smaller than the number of dikelets counted and the histogram in Figure 3 is likely a mixture of dikelets and half-dikelets. This interpretation is important for consideration of repeating seismic events; see Section 6 below.

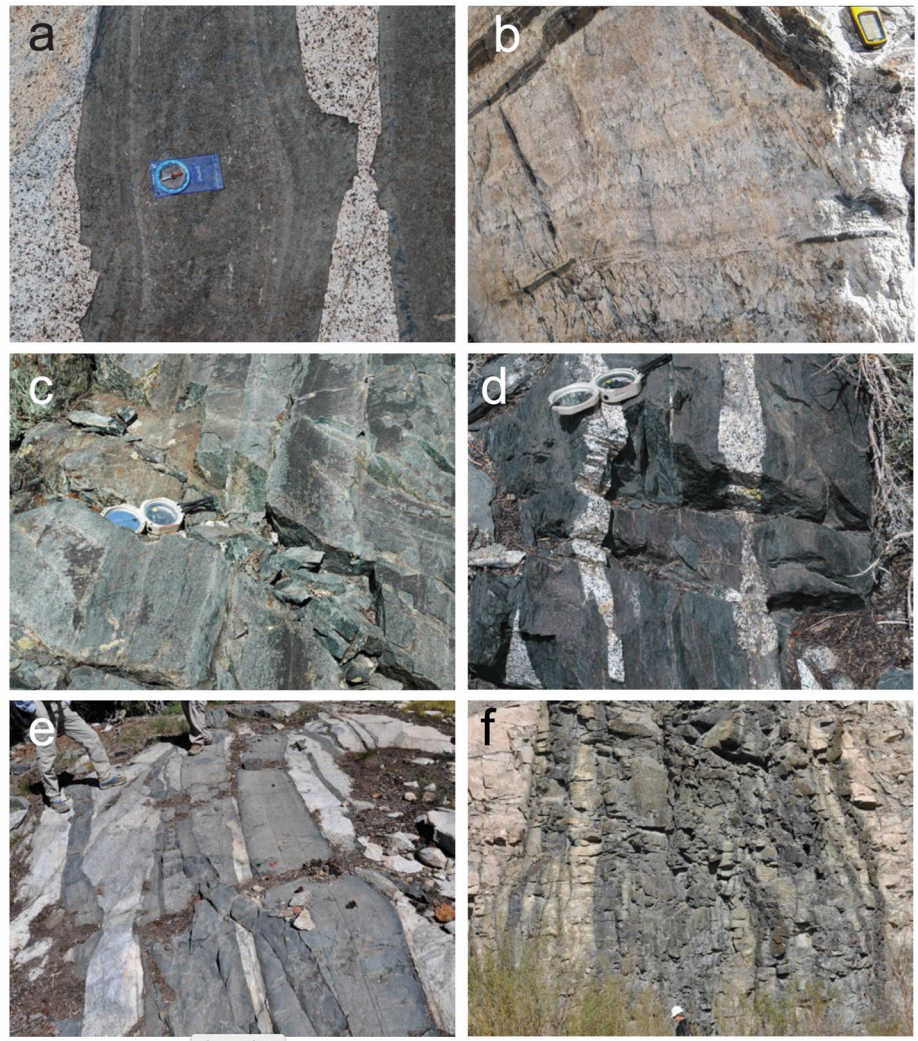

Figure 2. Composite dikes and their dikelets. (a) Composite dike consisting of an early pulse split down the middle by another (under compass; compass circle is 5 cm in diameter). (b) Composite aplite-pegmatite sill cutting the aureole of the Alta Stock, Utah. Black bands are thin sheets of schist. Width of field ~2 m. (c) Complex composite dike; boundaries of dikelets marked by grain-size changes. Compass is 10 cm in width. (d) Complex composite dike with isolated screens of host granodiorite. (e) Composite dikes cut by a dike that jumps from one to another. Feet for scale. (f) Quarry wall near Rocky Mount, North Carolina showing thick 200 Ma dikes composed of numerous dikelets. Person with hard hat for scale. Locations in photos (a) and (e) are along the John Muir Trail near Mt. Cedric Wright; (c) and (d) are from South Fork of Big Pine Creek, all in California.

2. Energy of Dike Injection

The moment (*N-m*; same units as energy) of a dike injection event can be estimated in a number of ways. Strengths and strain energies are discussed by Gudmundsson (2020). Here we consider dikes intruded at depths of a km or more, where open fractures cannot be sustained. In a compensated linear vector dipole (CLVD) mechanism the force system can be idealized as three orthogonal dipoles with moments of λ, λ, $\lambda + 2\mu$ (the latter perpendicular to the crack; Julian, 1983; Aki & Richards, 1980, Section 3.3). The moment of such an event can be expressed as:

$$M_o = V\left(\lambda + 2\mu\right) \tag{2}$$

where λ and μ are the first and second Lamé parameters and V is the volume of the injection. This is for the tensile crack portion of the CLVD. The Lamé parameters have units of stress. In addition, if fluid flow into the dike is

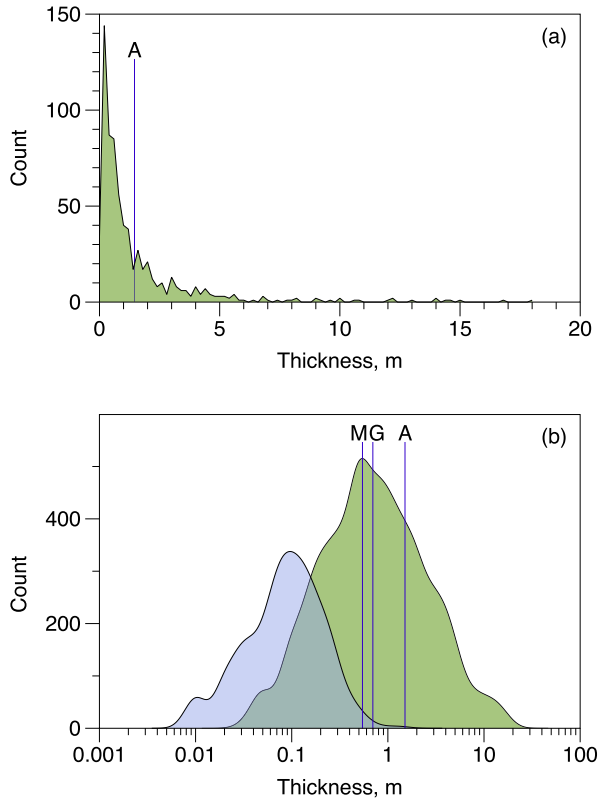

Figure 3. Thickness distribution of 705 dikes from the Independence swarm of eastern California; data from Bartley et al. (2007), Glazner et al. (2008), and this study. (a) Histogram of thicknesses showing that most dikes are on the order of ~1 m thick, but thicknesses of individual dikes range up to nearly 20 m. Arithmetic average (a) is difficult to discern from the distribution. (b) Histogram of $\log_{10}$ of thickness in meters of dikes (green) and dikelets (blue; $n = 287$). For the dikes, the mode (M) is 0.5 m, the geometric mean (M) is 0.7 m, and the arithmetic mean (a) is 1.5 m, a misleading measure of typical dike width. Geometric mean of dikelet distribution is 0.09 m.

equivalent to an isotropic implosion, (the magma chamber shrinks as magma moves from the chamber into the connected dike), then:

$$M_o = \frac{4}{3}\mu V \tag{3}$$

again following Julian (1983). This is the second part of the CLVD, required for conservation of mass; the geometry is shown in Figure 2a of Chouet (1996).

For earthquakes generated by wastewater injection, McGarr (2014) determined the relationship:

$$M_o = \mu V \tag{4}$$

All of these expressions estimate the maximum seismic moment that could be expected from a given injection event; actual radiated seismic energy is typically a small fraction of this (see below; Ágústsdóttir et al., 2016; McGarr & Barbour, 2018).

For comparison the scalar moment for typical shear event is:

$$M_o = A\bar{s}\mu \tag{5}$$

where A is the area over which slip occurs and $\bar{s}$ is the average slip distance. Area and slip maintain a constant ratio over many orders of magnitude. Note that $A\bar{s}$ has units of length cubed, the same as volume. The radiated seismic energy is also small, averaging a few percent (Scholz, 2019).

3. A Model Linking Dike Injection and *b*-Value

3.1. Exponentials

We propose that dike injection events trigger earthquakes, either directly by causing slip or opening on faults or indirectly by increasing stresses that are later relieved by nearby faults, and that the lognormal distribution of dike thicknesses (and by inference, volumes) produces a spectrum of earthquake magnitudes with *b*-values characteristic of volcanic areas. Two possibilities are most likely: (a) the dikes are adjacent to the shear fractures in which volcano-tectonic events occur, and (b) direct injection of magma may cause some of the low-frequency events in the dikes themselves.

3.2. Sampling Bias and True Dikelet Distribution

We make the usual assumption (e.g., Segall et al., 2001) that the dikes and dikelets fill coin-shaped cracks (Figure 4) with aspect ratios in the range of 10^2–10^3 (Rubin, 1995). Our sampling traverses represent an oriented random cut through such an array (Figure 4). This will lead to systematic undersampling of the smaller dikes, akin to undersampling smaller particles in a two-dimensional cut through a three-dimensional object (Glazner & Mills, 2012). As a result, the size distribution (Figure 4) will be skewed away from the thinner and therefore smaller dikes.

We examined this bias with Monte Carlo analysis using this procedure:

1. Generate 1 million dikelet widths and corresponding diameters drawn from a lognormal distribution fit to the field data in Figure 3.
2. Generate corresponding random dikelet centers in a cube whose dimensions are 10 times larger than the typical largest dike diameter; place dikes in cube parallel to one edge of the cube.
3. Calculate which dikes are intersected by a traverse (line) that runs through the center of the cube perpendicular to the dikes.

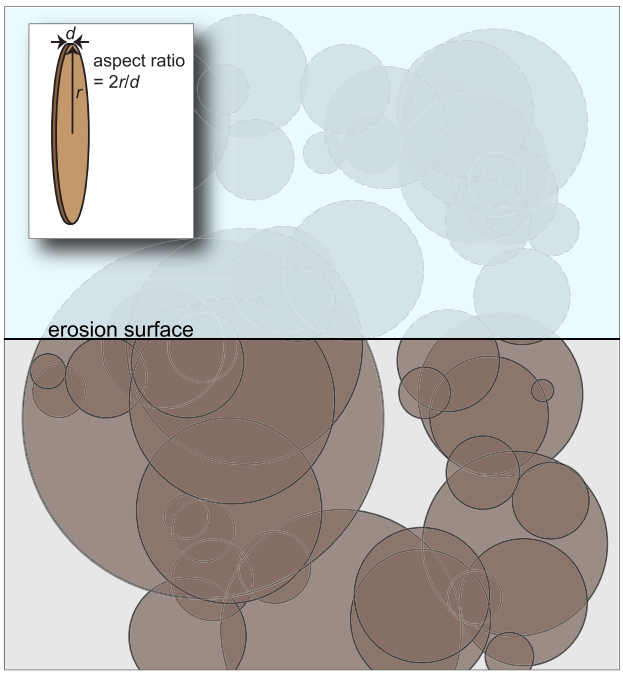

Figure 4. Highly schematic view perpendicular to a dike swarm intersecting an erosion surface. Dikes are idealized as coin-shaped cracks with constant aspect ratio. Only dikes that intersect the erosion surface are available to be measured, and thus smaller dikes are undersampled relative to larger ones. Undersampling shifts the distribution of measured dike thicknesses to greater values than those of the true distribution, but the variance of measured widths is similar to that of the true distribution.

4. Examine distribution of intersected dikelet widths. These prove to have a roughly lognormal distribution as well, with a similar standard deviation but higher mean owing to undersampling of smaller dikelets.
5. Adjust mean of input data downward and iterate until mean of intersected dikelets matches mean of observed dikelets.

Figure 5 shows the results of one such analysis. One million dikes with the specified lognormal mean and standard deviation generated 1,719 intersections with a mean equivalent to the observed dikelets. Conveniently, the lognormal standard deviation is essentially the same for both datasets.

4. The Model

The algorithm used to convert dike injection to *b*-value is as follows:

1. Generate n (typically 10^6) random dikelets with thicknesses d drawn from the lognormal distribution in Figure 3.
2. Censor the distribution by truncating the left side at $d = 0.01$ m, the thinnest dikelets observed.
3. Calculate the volume V of each dikelet assuming a given aspect ratio a (generally 1,000).
4. Calculate the moment of each dikelet-filling event using one of the relationships in Section 2 above. Results are insensitive to this choice (see below), so as a default we use Equation 2.
5. Multiply each geodetic moment by a constant (k, typically 0.01) that represents the fraction of geodetic moment that is converted to seismic moment.
6. Convert these numbers to moment magnitude using the relationship of Hanks and Kanamori (1979):

$$M = \left(log_{10}M_0 - 9.1\right) / 1.5 \tag{6}$$

7. Plot a cumulative magnitude-number diagram and estimate *b*.

In this algorithm the moment is thus given by

$$M_o = \frac{\pi}{4} k d^3 a^2 \left(\lambda + 2\mu\right) \tag{7}$$

5. Results

5.1. Calculated *b*-Value

In Equation 7, the terms making up the moment are multiplicative. Because the magnitude is proportional to the logarithm of the moment, changing any of the terms by a given factor shifts the resulting *b*-value curve laterally but does not change its slope. The only controls on the slope, and hence the *b*-value, in this model are the standard deviation of the lognormal distribution and the set of random dikelet thicknesses drawn from that distribution. The former is the primary slope control, and the latter introduces slight variability.

Results of several simulations are shown in Figure 6. The baseline model uses $k = 0.01$, $a = 1000$, $\mu = \lambda = 3 \times 10^{10}$ Pa, and lognormal mean (−3.9) standard deviation (0.94) from the Monte Carlo simulation of Section 4.2. In Figure 6a, the standard deviation was varied; this has a large effect on the slope of the curve. In Figure 6b, a set of 10,000 dike apertures was generated, and then the other model parameters save for the standard deviation were varied over 1–2 orders of magnitude. Values were drawn from distributions in which the logarithm of the parameter was uniformly distributed within these limits: a 100–1000, k 0.01–0.5, mean 0.01–0.2 m, μ and λ 10^9–10^{11} Pa. Over 1,000 model runs the maximum magnitude varies from ~1.8 to ~5, but the slopes of the curves are identical.

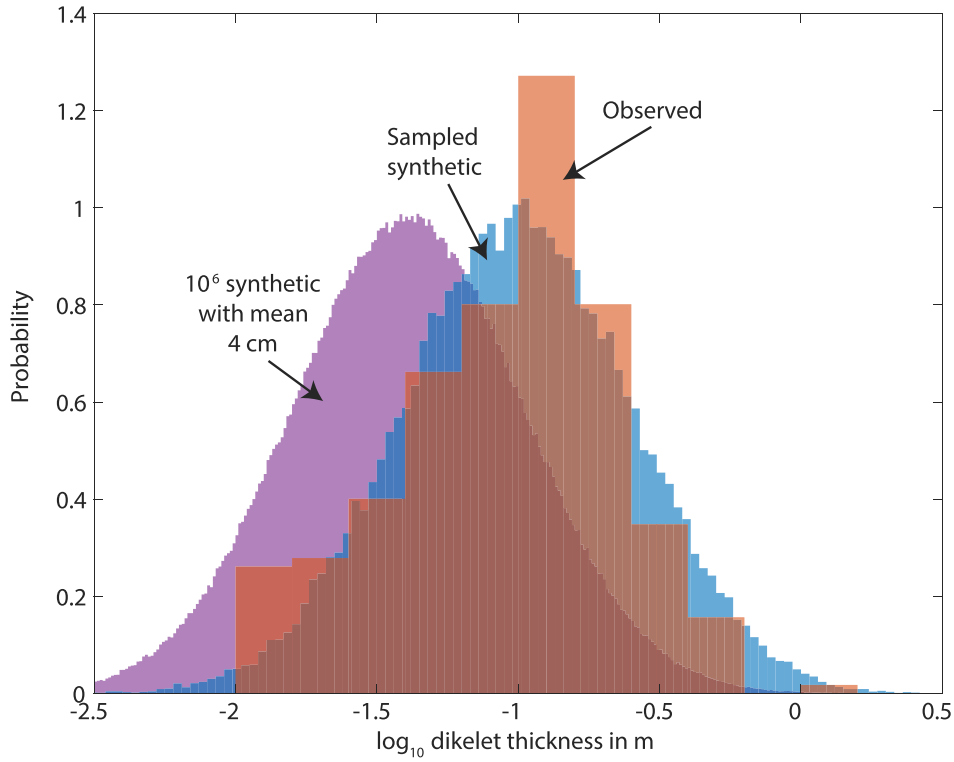

Figure 5. Monte Carlo simulation of dike sampling. Observed dikelet distribution has a lognormal mean of 0.08 m and a lognormal standard deviation of 2.56 m. To account for undersampling of smaller dikes, 10^6 synthetic dikelets with lognormal mean 0.04 m were generated and sampled by the algorithm described; this resulted in 1,719 surface intersections with the depicted distribution, which has the same mean and standard deviation as the observed distribution.

It is difficult to objectively determine a *b*-value from curves such as those in Figure 6 because there is gentle curvature throughout. The standard methods for estimating *b* involve the maximum likelihood method (Aki, 1965; Utsu, 1965), or weighted least squares (Bender, 1983). The benefits and limitations of various measurements are discussed by Guttorp (1987), Sandri and Marzocchi (2007) and others. Earthquake data (e.g., Figure 1) generally show slight curvature as well. In view of the difficulty of defining an objective way to estimate *b*, in Figure 6 we simply show representative slopes, allowing visual comparison of the simulation to earthquake plots.

The synthetic *b*-value from these simulations is ∼1.6–1.8, very much in the range of observed *b*-values from active volcanic areas (Table A1) and significantly higher than the $b = 1$ values that characterize tectonic earthquakes. In volcanic systems the mean for HF events is 1.13, close to the value for worldwide tectonic events, but the mean for LF events is 2.44. For HF events there are only a few *b*-values from 1.7 to 2.1, all from a single volcano (Table A1). For LF events there are numerous *b*-values at and near 1.7. Hence the simulation for dike swarms yields a synthetic *b*-value that is more consistent with the seismic *b*-values observed for LF events.

Our synthetic curves always fall off at lower magnitude. For real earthquake catalogs this is attributed to catalog incompleteness; smaller earthquakes are less likely to be recorded. If our model bears any relationship to reality then this fall-off might also result from the lognormal distribution of dike thicknesses. Rather than following a power-law distribution, as proposed by Gudmundsson (1995) for Iceland dikes, the frequency of small dikes falls off rapidly at values smaller than the median (Krumbholz et al., 2014). This is likely a result of the thermomechanical difficulty of propagating thin dikes; Rubin (1995) showed that the propagation distance of a freezing dike should scale with the fourth power of the dike aperture.

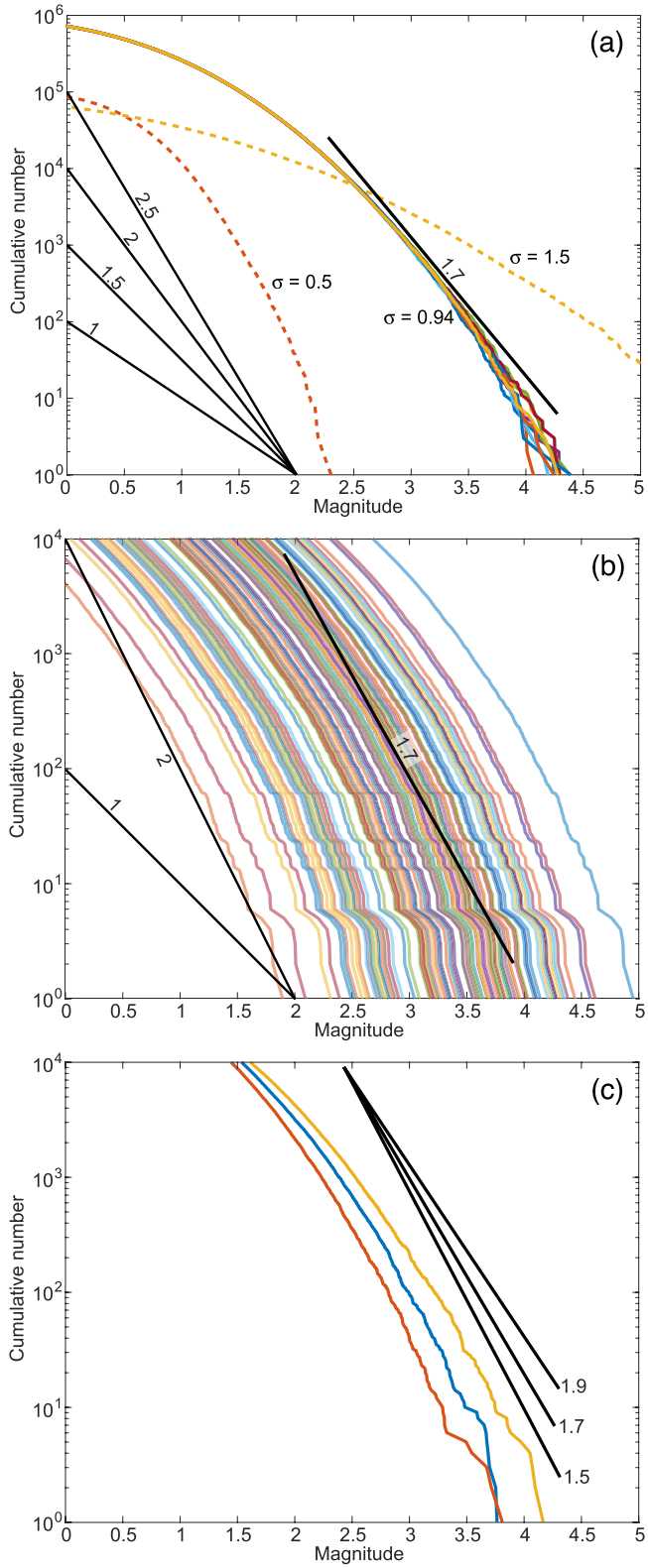

Figure 6. (a) 10 simulations of 10^6 dikelets (solid lines), generated using the thickness distribution of Figure 3 and $k = 0.01$. The linear portions of the curves have slopes of ~1.7, similar to those of active volcanic areas. Dashed curves show the effect of changing the lognormal standard deviation on the calculated value; b depends strongly on this value. (b) One hundred simulations with the same standard deviation but large variations in elastic parameters, k, and the lognormal mean; b is invariant under these variations. (c) Three simulations using observed lognormal standard deviation ±2 bootstrap standard deviations (see text).

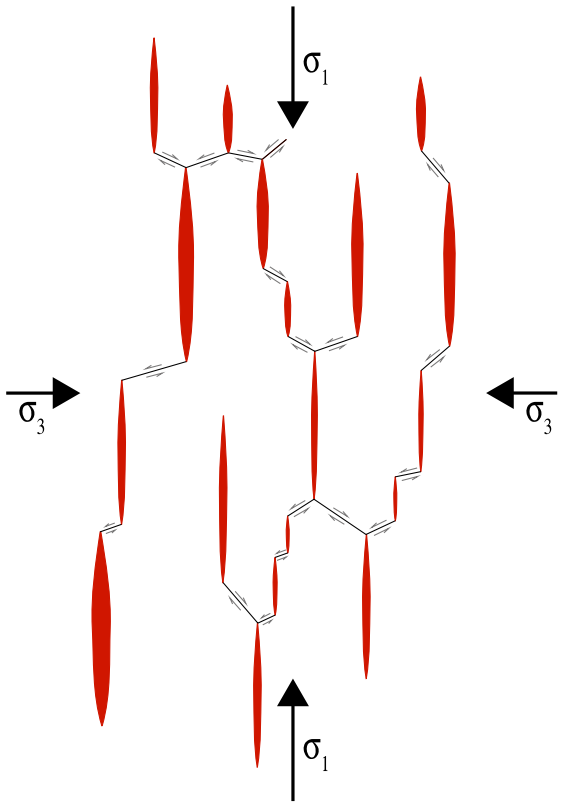

Figure 7. Hill (1977)'s fracture-mesh model of magmatic earthquake swarms. Dikes oriented with their planes perpendicular to the least compressive stress are linked by conjugate fault planes that accommodate dilation. Filling the dikes provides elastic stress that is relieved by earthquakes on the faults.

5.2. Sensitivity Analysis: It is All in the Standard Deviation

There are a number of parameters that go into the model. These are the mean of the lognormal distribution, standard deviation of the lognormal distribution, fraction (k) of dike-filling moment that is converted to seismic moment, dikelet aspect ratio, and elastic constants.

We explored a wide range of these parameters (Figure 6b) and found that only the variance affects the slope. The other parameters all move the curve left or right but do not affect the slope. For example, increasing the aspect ratio increases the volume of each dike, producing larger calculated seismic moments; this shifts the curve to the right. Similarly, changing elastic constants changes only the calculated magnitudes, shifting the curve left or right. The standard deviation of the lognormal distribution is the only variable that affects the slope of the cumulative number-magnitude plot, and hence the b-value.

As our observations of dikelet thickness distribution are limited to a single data set, we used the bootstrap method to estimate the sampling distribution of the lognormal standard deviation. One thousand resamplings and calculations of the lognormal standard deviation yield a mean of 0.94 and a standard deviation of 0.038. Figure 6c shows that propagating twice the standard deviation through the Monte Carlo simulation changes estimated b by $\sim\pm0.2$.

For reasonable parameter choices (e.g., Figure 6) the calculated earthquake magnitudes are in the realm of observation, and for the observed dikelet thickness variance, the calculated b-value (1.7) is right in the range of observation in volcanic areas (see Table A1). Our model, which is essentially a one-parameter model, matches observations remarkably well.

6. Discussion

Seismic moment in volcanic areas is typically a small fraction (perhaps 1%) of geodetic moment (Ágústsdóttir et al., 2016; Grandin et al., 2009; McGarr & Barbour, 2018). Thus, much dike injection is accomplished aseismically. However, it is likely that dike filling produces elastic strain in surrounding rocks that is relieved by earthquakes, and thus the volume of dike-filling events should scale with earthquakes produced by those dike-filling events. Regardless of the exact ratios between volume and number of earthquakes, the scaling, or ratio of small to large events, remains the same.

The fracture-mesh model of Hill (1977), shown in Figure 7 and commonly invoked in seismic swarms (e.g., Toda et al., 2002), is consistent with this hypothesis. Filling of cracks with magma contributes to overall volume increase and thus geodetic moment, but only a fraction of this energy is radiated as seismic energy, the rest being taken up by creep or subseismic slip on fractures. The Independence swarm is associated with a dense network of small-displacement shear zones that are kinematically linked. Wall rock markers cut by west-northwest-striking dikes and shear zones consistently have left-lateral separation, whereas north-striking shear zones and rare north-striking dikes consistently have right-lateral separation (Glazner et al., 1999). These are all consistent with a stress field in which the greatest compressive stress was oriented approximately northeast-southwest (Bartley et al., 2012).

The magnitude range for the modeling is similar to the magnitude range for volcanic earthquake swarms as determined for a sample of 600 swarms by Benoit and McNutt (1996). Most of these reported magnitudes but only a few reported b-values, so we performed a separate compilation of 61 b-values from 44 volcanoes. Seismic magnitude estimates for events in Figure 6 above range from 0 to 5, which is in the same range as observations at dozens of volcanoes.

As stated previously, durations of contemporary volcanic swarms range from hours to years with a geometric mean of 5.5 days. Swarms of LF events are generally shorter and those for HF events are longer. These are quite

short in terms of geologic time. We can make a case that LF event swarms are a closer analog for the emplacement of dikes, but this is an inference only. Further, volcanic areas have repeated swarms at many time scales, so the geologic dike swarm may represent many seismic swarms. It is difficult to estimate the durations of events that produce dike swarms, but evidence for dike splitting (Section 1.4) suggests that dikes composed of many dikelets develop during the cooling time of individual dikes, e.g., days to months or years depending on the depth and thus ambient temperature. We suggest these are in reasonable agreement with independent data on the occurrence of volcanic earthquake swarms at many different volcanoes.

There are many cases in the literature of repeating LF events at volcanoes (e.g., Buurman et al., 2013; Johnson et al., 2010; Massin et al., 2013; Park et al., 2019; Petersen, 2007). That is, tens to thousands of events are observed with nearly identical waveforms. An idea for these is that they represent a non-destructive and repeating source, such as rapid or jerky dike opening followed by relaxation (Tuffen et al., 2003). Thus, the same physical source may be responsible for many seismic events.

Some dikes show evidence for reuse or multiple dikelets (Figure 2). However, the exact number of re-use events cannot be determined from geologic evidence alone. This may help explain part of the roll-off at the left of Figure 6. It is known that the Gutenberg-Richter relation for seismic events holds all the way down to laboratory scale (Kwiatek et al., 2010).

Turcotte (1992) explored the relation of the frequency-magnitude relation for earthquakes versus the fractal dimension. Using his equation, which includes some simplifying assumptions (Turcotte, 1992, page 37, equation 4.10), the fractal dimension is two times the b-value ($D = 2b$). This has a ready interpretation in that the fractal dimension of 2 for typical tectonic $b = 1$ implies that $D = 2$ so the fault is a planar surface.

A value for b of 1.5 would then suggest $D = 3$, implying that the source is a volume such as a dike, which would be appropriate for volcanic sources. For $b > 1.5$, $D > 3$, which is a non-physical dimension. The simplest way to reconcile this would be for the sources to reuse the same volumes. This notion is compatible with seismic observations of repeating earthquakes and non-destructive sources, as noted above.

The average b-value for volcanoes is 1.7, as determined by us (Table A1) and independently by Roberts et al. (2015). Thus, based on the discussion above, the fractal dimension would be $2b$ or 3.4. This implies a volume source with a small degree of reuse. The equivalent b-value based on our dike observations and modeling is also 1.7. While this could be coincidence, we suggest that common conditions are responsible for both. We infer that the most likely explanation is the distribution of fractures and joints, which are pervasive at volcanoes. Cooling cracks, in particular, are numerous and small scale. These would give many small sources for both dike paths (e.g., Gudmundsson, 2020) and earthquake sources. This observation links physical sources with their size distribution, which for $b = 1.7$ implies many small sources. Note that the dikes and earthquakes need not be simultaneous or directly related; the earthquakes may occur in wall rocks and dike growth itself may be aseismic. But rather, both phenomena take advantage of the same availability of fractures in the immediate vicinity.

Overall, there is reasonable agreement between the geologic (spatial) and seismic (temporal) observations. Although previously these have been two separate suites of observations by geologists and seismologists, respectively, we suggest these are linked and provide a plausible explanation. The earthquake swarms are the seismic expression of dike injections, and conversely, the dike swarms are the geologic expression of the transient seismic processes associated with magma injection.

7. Conclusions

We studied, and compared quantitatively, dike swarms and volcanic earthquake swarms. For dike distribution we used the Independence dike swarm in California, which has outstanding glacially polished exposure and enough dikes to form a robust sample. For seismic b-values, we compiled our own worldwide sample of 61 cases at 44 volcanoes. This is also a robust sample, is similar to other data sets, and includes many examples for which the plots are quite linear. The average b-value at volcanoes is 1.7. To establish links between the dikes (spatial) and earthquake swarms (temporal) we performed Monte Carlo simulations of dike distributions and sampling. The modeling uses a simple and straightforward approach. Theoretical distributions of the sizes of dikes from the model yield plots with slopes similar to the b-value plots; these also have slopes of ~1.7. The exact details of M_o

calculations used for these plots are less important than the variance. We infer that high fracture density, such as from cooling cracks, in the vicinity of volcanoes, may contribute to the high and common *b*-values observed.

Appendix A: Compilation of *b*-Values.

We compiled Table A1 of *b*-values at volcanoes for comparison with the dike size distributions. The table has three sections. Prior to 1995, seismic events were sorted by type, such as A or B-type (Minakami, 1960), and generally a single *b*-value calculation was made for each. Starting in 1997, spatial analyses of *b*-values were made at a number of volcanoes by Wiemer and colleagues (see Table A1 for references). These lumped all the seismic events together and determine *b*-values at pre-defined spatial grid points. An example is shown in Figure A1. About a dozen such studies have shown two high-*b* anomalies, one at presumed depths of magma chambers (7–12 km) and a second shallower anomaly at depths of 3–4 km. We also added some recent examples of b-value determinations in a third section of the table.

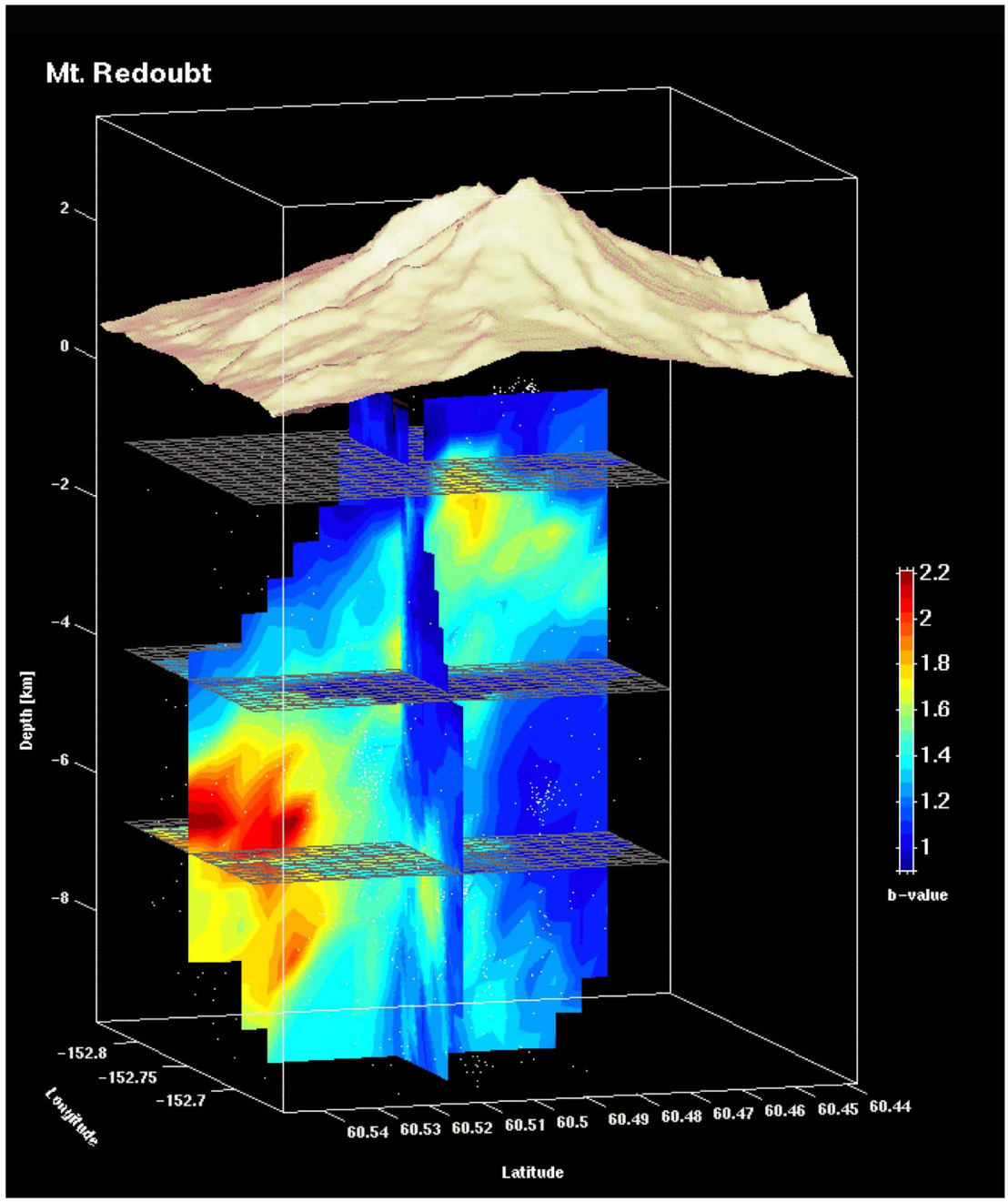

Figure A1. Spatial *b*-value calculations for Redoubt volcano. The *b*-value is calculated using the 100 nearest earthquakes for each point in a 3-D grid. Colors represent the *b*-value. Note the high *b* anomalies at 2 and 6–10 km. Figure courtesy of S. Wiemer (writ. comm.).

To make the table we compiled the *b*-values into several groups, and prepared histograms. The *b*-values were sorted into bins of width 0.1, using single values as appropriate and using one value per bin when a range was given. For example, a range in *b* from 1.4 to 1.9 would have one value each for bins 1.4, 1.5, 1.6, 1.7, 1.8, and 1.9. Four histograms were prepared (Figure A2). The first (Figure A2 part a) shows HF events from the first part of Table A1. It has a range of *b* from 0.5 to 2.1 and a mean of $b = 1.13$. This is slightly higher than the worldwide average for tectonic shocks of $b = 0.9$–1.0. The second (Figure A2 part b) is similar but shows data from LF events from the first part of Table A1. These data have a range from 1.4 to 3.7 and a mean of $b = 2.44$. This a representative value for LF events. The third histogram (Figure A2 part c) shows the range of values using data

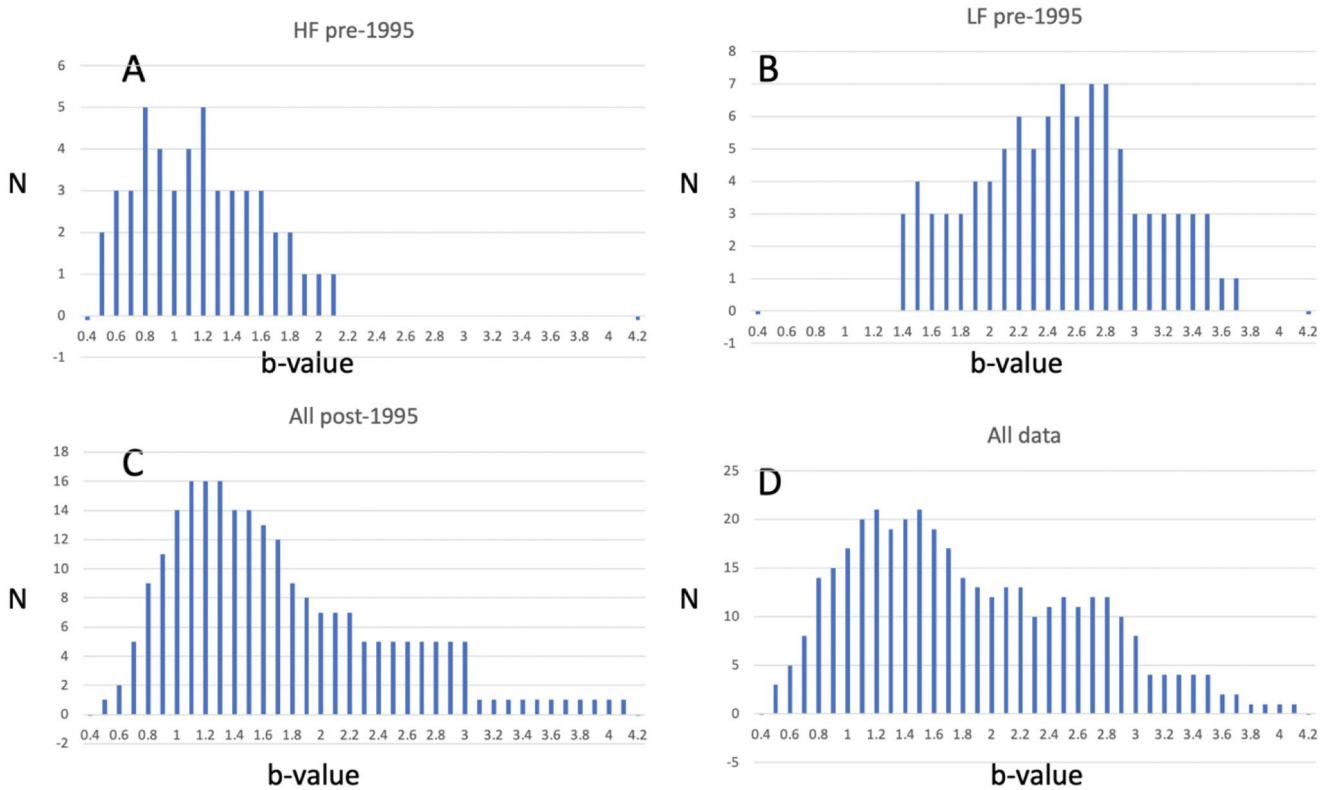

Figure A2. Histograms of *b*-value distributions. *N* is number of observations. *b*-values are in bins of width 0.1.

after 1997; event types were not distinguished and likely included both HF and LF events. Here the range is from 0.5 to >4.1 and the mean is $b = 1.71$. The fourth histogram (Figure A1 part D) shows all the data combined. It has a range from 0.5 to >4.1 and a mean of $b = 1.83$. Note that the average of the HF and LF events (Figure A2 parts A and B) is $b = \sim 1.85$. All these seismic *b*-values are remarkably close the geologic value of $b = 1.7$ determined for the Independence dike swarm. Note that we did not use the recent values (third part of Table A1) to make the histograms. The samples from parts one and two are already large and robust. Further, we note that the compilation of Roberts et al. (2015) found a peak in the data at $b = 1.7$, similar to our results. There is partial overlap in data from Roberts et al. (2015) and our compilation. All the samples are large and likely representative.

Table A1
Compilation of b-Values at Volcanoes

Volcano	Event type	*b*	Depth, km	Comment	Reference
				Pre-1995	
Asama	B	1.8–3.5			Minakami (1960)
Aso	A	0.8–0.9			Minakami (1960)
Ebino 1968-69	A	1.5			Minakami (1974)
Erebus	LF	1.4–1.6			Dibble et al. (1984)
Fuego	A	0.7–2.1			Yuan et al. (1984)
Fuego June 1973	A	1.25			McNutt and Harlow (1983)
Etna	B	2.4–3.7			Gresta and Patanè (1983)
Hakone 1959-60	A	1.6			Minakami (1974)
Hengill	HF	0.5–1.0		Includes nondouble couple	Foulger (1988)

Table A1
Continued

Volcano	Event type	*b*	Depth, km	Comment	Reference
Hukui 1948	A	1.2			Minakami (1974)
Izalco	B	1.7			McNutt and Harlow (1983)
Kilauea	LP	1.5–2.5			Koyanagi et al. (1988)
Kilauea Iki lava lake	Cooling cracks	2.23			Peck and Minakami (1968)
Kusatsu-sirane	A	0.8	deep		Minakami et al. (1969)
Kusatsu-sirane	A	1.8	shallow		Minakami et al. (1969)
Kutinoerabu	B	1.4			Minakami et al. (1969)
Matsushiro	A	1.1			Minakami (1974)
Mount St Helens	A	0.6			Endo et al. (1981)
Mount St Helens	B	2.77			Endo et al. (1981)
Mount St Helens	all	0.5–1.75			Main (1987)
Pacaya	B	2.88			McNutt and Harlow (1983)
Pavlof	B	1.9–2.6			McNutt (1986)
Redoubt	VT	1.1–1.4			Lahr et al. (1994); K. Wolf, writ. comm., 1994
Redoubt	LP	1.4–2.9			Lahr et al. (1994); K. Wolf, writ. comm., 1994
Ruapehu	LF	1.5			Latter (1979), (1981)
Sakurajima	B	2.5–3.5			Minakami (1974)
Sakurajima	explosion	2.9			Minakami (1974)
San Cristobal	B	2.73			McNutt and Harlow (1983)
Stromboli	LF	2.8			Lo Bascio et al. (1973)
Usu	B	2.1–2.8			Minakami (1960)
hydrofracturing	Acoustic emissions	1–1.5			Tsukahara and Ikeda (1987)
				Post-1997	
Mount St Helens 1988-1996	all	0.8–1.4	2.6–4.3		Wiemer and McNutt (1997)
Mount St Helens 1988-1996	all	0.84–1.4	5.8–8		Wiemer and McNutt (1997)
Mount Spurr	all	0.74–1.17	2–4.8		Wiemer and McNutt (1997)
Mount Spurr	all	0.74–1.03	11+		Wiemer and McNutt (1997)
Mammoth Mountain	all	1.0–1.6	4.5–5.5		Wiemer et al. (1998)
Mammoth Mountain	all	1.1–1.8	7.0–9.0		Wiemer et al. (1998)
Pinatubo	all	1.26–1.5	0–3.8		Sánchez et al. (2004)
Pinatubo	all	1.16–1.38	8.5–12		Sánchez et al. (2004)
Montserrat	all	0.92–3.07	0–4	EC, CP, GS	Power et al. (1998)
Montserrat	all	0.92–3.07	0–2	EC, CP, GS	Power et al. (1998)
Off-ito	all	0.7–1.5	7–15		Wyss et al. (1997)
Etna	all	1.5–3	1–5	WSW	Murru et al. (1999)
Etna	all	1.5–3	7–13		Murru et al. (1999)
Kilauea ERZ	all	0.8–1.3	4–8		Wyss et al. (2001)
Kilauea	all	0.52–1.73	5–7		Wyss et al. (2001)
Mount Mageik	all	1.04–4.46	0–4		Jolly et al. (2007)
Makushin	all	0.8–1.9	1–3		Bridges and Gao (2006)
Coso	all	1.7	0.8–3		M. Wyss, pers. comm.

Table A1
Continued

Volcano	Event type	*b*	Depth, km	Comment	Reference
Long Valley	all	0.6–2.2	1–11	Resurgent dome	Wiemer et al. (1998)
Katmai	all	1.02–1.71	0–5	Trident-Mageik	Jolly et al. (2007)
Usu	all	1.1–2.2			Suzuki and Kasahara (1980)
				Selected additions	
Santorini	all	0.9–1.47			Chouliaras et al. (2012)
Kirishima	all	0.57–1.4			Chiba and Shimizu (2018)
Yellowstone	all	0.5–1.5		swarms	Farrell et al. (2009)
Askja and Bardarbunga	all	0.998–1.51		Four groupings	Greenfield et al. (2020)
El Hierro	all	1.12–2.25 (0.67)*		Early and eruptive phases; *Using MLM	Ibáñez et al. (2012)
Augustine	all	0.781–1.85		Pre and syn-eruptive	Jacobs and McNutt (2010)
Copahue	all	0.7, >1.2		Magmatic and hydrothermal	Lazo et al. (2015)
Popocateptl	all	1.56–1.92			Novelo-Casanova et al. (2006)
various	all	0.5–3.5		34 examples from 21 volcanoes; peak at $b = 1.7$	Roberts et al. (2015)
Aluto	all	0.82–2.25	−2–9 km	Three depth intervals	Wilks et al. (2017)

There are two questions before us: (a) which depth range is most suitable for comparison of seismic *b* to dike distribution? And (b) which type of events should be used for comparison? For the first question, we infer that the deeper events are more likely representative of the dike formation. For the second, we suggest that the combined events are best for comparison. That is, a suite of seismic events including both HF and LF events appears to be associated with dike formation. The seismic and geologic parts share common scaling relations.

Data Availability Statement

Data in Table S1 are archived at the EarthChem Library: Glazner, A., Bartley, J., Coleman, D., 2020. Thicknesses of dikes and dikelets in the Independence dike swarm, California, Version 1.0. Interdisciplinary Earth Data Alliance (IEDA). https://doi.org/10.26022/IEDA/111809. Accessed 2020-12-28.

Acknowledgments
The authors thank those behind the 2018 Chapman Conference on Merging Geophysical, Petrochronologic, and Modeling Perspectives of Large Silicic Magma Systems, especially Brad Singer, for a stimulating meeting, spectacular field trip, and delicious pisco sours. Thorough and thoughtful comments by reviewers Agust Gudmundsson and Chet Hopp and by Editor Rachel Abercrombie were extremely helpful to our revisions. Jamie Farrell graciously shared his expertise and data on Yellowstone seismic swarms. Stefan Wiemer shared the figure shown in the appendix as Figure A1. Special thanks to John Bartley, Drew Coleman, and Kurt Frankel, with whom AFG spent many arduous days measuring dikes and dikelets. Tyler Benton's senior thesis work clearly showed the composite nature of dikes such as those in Figure 1. Research was supported by the Geothermal Program Office of the China Lake Naval Air Warfare Center contract N68936-01-C-0090, the Mary Lily Kenan Flagler Bingham Professorship, and NSF grants EAR-9526803 and EAR-9814789.

References

Ágústsdóttir, T., Woods, J., Greenfield, T., Green, R. G., White, R. S., Winder, T., et al. (2016). Strike-slip faulting during the 2014 Bárðarbunga-Holuhraun dike intrusion, central Iceland. *Geophysical Research Letters*, *43*, 1495–1503.

Aki, K. (1965). Maximum likelihood estimate of b in the formula log N= a-bM and its confidence limits. *Bulletin of the Earthquake Research Institute, University of Tokyo*, *43*, 237–239.

Aki, K., & Richards, P. G. (1980). *Quantitative seismology: Theory and methods*. Freeman and Co.

Bartley, J. M., Glazner, A. F., Coleman, D. S., Kylander-Clark, A., Mapes, R., & Friedrich, A. M. (2007). Large Laramide dextral offset across Owens Valley, California, and its possible relation to tectonic unroofing of the southern Sierra Nevada. *Special Papers - Geological Society of America*, *434*. https://doi.org/10.1130/2007.2434(07).c.

Bartley, J. M., Glazner, A. F., & Mahan, K. H. (2012). Formation of pluton roofs, floors, and walls by crack opening at Split mountain, Sierra Nevada, California. *Geosphere*, *8*(5), 1086–1103. https://doi.org/10.1130/GES00722.1

Belachew, M., Ebinger, C., & Coté, D. (2013). Source mechanisms of dike-induced earthquakes in the Dabbahu-Manda Hararo rift segment in Afar, Ethiopia: Implications for faulting above dikes. *Geophysical Journal International*, *192*(3), 907–917. https://doi.org/10.1093/gji/ggs076

Bender, B. (1983). Maximum likelihood estimation of b values for magnitude grouped data. *Bulletin of the Seismological Society of America*, *73*(3), 831–851. https://doi.org/10.1785/bssa0730030831

Benoit, J. P., & McNutt, S. R. (1996). Global volcanic earthquake swarm database and preliminary analysis of volcanic earthquake swarm duration. *Annali di Geofisica*, *39*(2), 221–229. https://doi.org/10.4401/ag-3963

Benton, T. J., Gaynor, S., & Glazner, A. F. (2011). Testing composite dike intrusion models with chemical analysis. *Abstracts with Programs - Geological Society of America*, *43*(4), 68.

Bridges, D. L., & Gao, S. S. (2006). Spatial variation of seismic b-values beneath Makushin Volcano, Unalaska Island, Alaska. *Earth and Planetary Science Letters*, *245*, 1408–2415. https://doi.org/10.1016/j.epsl.2006.03.010

Buurman, H., West, M. E., & Roman, D. C. (2013). Using repeating volcano-tectonic earthquakes to track post-eruptive activity in the conduit system at Redoubt Volcano, Alaska. *Geology*, *41*(4), 511–514. https://doi.org/10.1130/g34089.1

Carl, B. S., & Glazner, A. F. (2002). Extent and significance of the Independence dike swarm, eastern California. *Memoirs - Geological Society of America*, *195*, 117–130. https://doi.org/10.1130/0-8137-1195-9.117

Chiba, K., & Shimizu, H. (2018). Spatial and temporal distributions of b-value in and around Shinmoe-dake, Kirishima volcano, Japan. *Earth, Planets and Space*, *70*, 1–9. https://doi.org/10.1186/s40623-018-0892-7

Chouet, B. A. (1996). New methods and future trends in seismological volcano monitoring. *Monitoring and mitigation of volcano hazards* (pp. 23–97). https://doi.org/10.1007/978-3-642-80087-0_2

Chouliaras, G., Drakatos, G., Makropoulos, K., & Melis, N. S. (2012). Recent seismicity detection increase in the Santorini volcanic island complex. *Natural Hazards and Earth System Sciences*, *12*, 859–866. https://doi.org/10.5194/nhess-12-859-2012

Coetzee, A., & Kisters, A. (2016). The 3D geometry of regional-scale dolerite saucer complexes and their feeders in the Secunda Complex, Karoo Basin. *Journal of Volcanology and Geothermal Research*, *317*, 66–79. https://doi.org/10.1016/j.jvolgeores.2016.04.001

Delaney, P. T., & Gartner, A. E. (1997). Physical processes of shallow mafic dike emplacement near the San Rafael Swell, Utah. *The Geological Society of America Bulletin*, *109*(9), 1177–1192. https://doi.org/10.1130/0016-7606(1997)109<1177:pposmd>2.3.co;2

Dibble, R. R., Kienle, J., Kyle, P. R., & Shibuya, K. (1984). Geophysical studies of Erebus volcano, Antarctica, from 1974 December to 1982 January. *New Zealand Journal of Geology and Geophysics*, *27*(4), 425–455. https://doi.org/10.1080/00288306.1984.10422264

Endo, E. T., Malone, S. D., Noson, L. L., & Weaver, C. S. (1981). Locations, magnitudes, and statistics of the March 20–May 18 earthquake sequence. *U. S. Geological Survey Professional Paper*, *1250*, 93–107.

Ernst, R. E., Buchan, K. L., Mahoney, J. J., & Coffin, M. F. (Eds.), (1997). Giant radiating dyke swarms; their use in identifying pre-Mesozoic large igneous provinces and mantle plumesLarge igneous provinces; continental, oceanic, and planetary flood volcanism. *Geophysical Monograph*, *100*, 297–333.

Ernst, R. E., Head, J. W., Parfitt, E., Grosfils, E., & Wilson, L. (1995). Giant radiating dyke swarms on Earth and Venus. *Earth-Science Reviews*, *39*(1–2), 1–58. https://doi.org/10.1016/0012-8252(95)00017-5

Farrell, J., Husen, S., & Smith, R. B. (2009). Earthquake swarm and b-value characterization of the Yellowstone volcano-tectonic system. *Journal of Volcanology and Geothermal Research*, *188*, 1260–3276. https://doi.org/10.1016/j.jvolgeores.2009.08.008

Farrell, J., Smith, R. B., Taira, T., Chang, W.-L., & Puskas, C. M. (2010). Dynamics and rapid migration of the energetic 2008-2009 Yellowstone Lake earthquake swarm. *Geophysical Research Letters*, *37*(19). https://doi.org/10.1029/2010GL044605

Foulger, G. R. (1988). Hengill triple junction, SW Iceland 1. Tectonic structure and the spatial and temporal distribution of local earthquakes. *Journal of Geophysical Research*, *93*(B11), 13493–13506. https://doi.org/10.1029/jb093ib11p13493

Frohlich, C., & Davis, S. D. (1993). Teleseismic b values; or, much ado about 1.0. *Journal of Geophysical Research*, *98*. https://doi.org/10.1029/92JB01891

Galerne, C. Y., Galland, O., Neumann, E. R., & Planke, S. (2011). 3D relationships between sills and their feeders: Evidence from the Golden Valley Sill Complex (Karoo Basin) and experimental modelling. *Journal of Volcanology and Geothermal Research*, *202*(3–4), 189–199. https://doi.org/10.1016/j.jvolgeores.2011.02.006

Glazner, A. F., Bartley, J. M., & Carl, B. S. (1999). Oblique opening and noncoaxial emplacement of Jurassic Independence dike swarm, California. *Journal of Structural Geology*, *21*(10), 1275–1283. https://doi.org/10.1016/s0191-8141(99)00090-5

Glazner, A. F., Carl, B. S., Coleman, D. S., Miller, J. S., & Bartley, J. M. (2008). Chemical variability and the composite nature of dikes from the Jurassic independence dike swarm, eastern California. *Special Papers - Geological Society of America*, *438*. https://doi.org/10.1130/2008.2438(16).c.

Glazner, A. F., & Mills, R. D. (2012). Interpreting two-dimensional cuts through broken geologic objects: Fractal and non-fractal size distributions. *Geosphere*, *8*(4). https://doi.org/10.1130/GES00731.1

Grandin, R., Socquet, A., Binet, R., Klinger, Y., Jacques, E., De Chabalier, J. B., et al. (2009). September 2005 Manda hararo-dabbahu rifting event, Afar (Ethiopia): Constraints provided by geodetic data. *Journal of Geophysical Research*, *114*(8). https://doi.org/10.1029/2008JB005843

Greenfield, T., & White, T. (2020). Seismicity of the Askja and Bárðarbunga volcanic systems of Iceland, 2009–2015. *Journal of Volcanology and Geothermal Research*, *391*, 106432. https://doi.org/10.1016/j.jvolgeores.2018.08.010

Gresta, S., & Patanè, G. (1983). Variation of b values before the Etnean eruption of March 1981. *Pure and Applied Geophysics*, *121*(2), 287–295. https://doi.org/10.1007/bf02590139

Gudmundsson, A. (1995). Infrastructure and mechanics of volcanic systems in Iceland. *Journal of Volcanology and Geothermal Research*, *64*, 1–22. https://doi.org/10.1016/0377-0273(95)92782-q

Gudmundsson, A. (2020). *Volcanotectonics: Understanding the structure, deformation, and dynamics of volcanoes* (p. 586). Cambridge University Press.

Gutenberg, B., & Richter, C. (1954). *Seismicity of the earth and associated phenomena*.

Guttorp, P. (1987). On least-squares estimation of b values. *Bulletin of the Seismological Society of America*, *77*(6), 2115–2124.

Hanks, T. C., & Kanamori, H. (1979). A moment magnitude scale. *Journal of Geophysical Research*, *84*(B5), 2348–2350. https://doi.org/10.1029/jb084ib05p02348

Hill, D. P. (1977). A model for earthquake swarms. *Journal of Geophysical Research*, *82*(8), 1347–1352. https://doi.org/10.1029/jb082i008p01347

Holtkamp, S. G., & Brudzinski, M. R. (2011). Earthquake swarms in circum-Pacific subduction zones. *Earth and Planetary Science Letters*, *305*(1–2), 215–225. https://doi.org/10.1016/j.epsl.2011.03.004

Huang, J., & Turcotte, D. L. (1988). Fractal distributions of stress and strength and variations of b-value. *Earth and Planetary Science Letters*, *91*(1–2), 223–230. https://doi.org/10.1016/0012-821X(88)90164-1

Ibáñez, J. M., De Angelis, S., Díaz-Moreno, A., Hernández, P., Alguacil, G., Posadas, A., Pérez, N. (2012). Insights into the 2011–2012 submarine eruption off the coast of El Hierro (Canary Islands, Spain) from statistical analyses of earthquake activity. *Geophysical Journal International*, *1912*, 659–670.

Ishimoto, M., & Iida, I. (1939). Observations of earthquakes registered with the microseismograph constructed recently (in Japanese with French abstract). *Bulletin of the Earthquake Research Institute*, *17*, 443–478.

Jacobs, K. M., & McNutt, S. R. (2010). Using seismic b-values to interpret seismicity rates and physical processes during the preeruptive earthquake swarm at Augustine Volcano 2005-2006. *The 2006 Eruption of Augustine Volcano, Alaska*. U.S. Geological Survey (pp. 1–17).

Johnson, J. H., Prejean, S., Savage, M. K., & Townend, J. (2010). Anisotropy, repeating earthquakes, and seismicity associated with the 2008 eruption of Okmok volcano, Alaska. *Journal of Geophysical Research*, *115*(B9). https://doi.org/10.1029/2009jb006991

Jolly, A. D., Moran, S. C., McNutt, S. R., & Stone, D. B. (2007). Three-dimensional P-wave velocity structure derived from local earthquakes at the Katmai group of volcanoes, Alaska. *Journal of Volcanology and Geothermal Research*, *159*(4), 326–342. https://doi.org/10.1016/j.jvolgeores.2006.06.022

Jolly, R. J. H., & Sanderson, D. J. (1995). Variation in the form and distribution of dykes in the Mull swarm, Scotland. *Journal of Structural Geology*, *17*(11), 1543–1556. https://doi.org/10.1016/0191-8141(95)00046-g

Julian, B. R. (1983). Evidence for dyke intrusion earthquake mechanisms near Long Valley caldera, California. *Nature*, *303*, 323–325. https://doi.org/10.1038/303323a0

King, G. (1983). The accommodation of large strains in the upper lithosphere of the earth and other solids by self-similar fault systems: The geometrical origin of b-value. *Pure and Applied Geophysics PAGEOPH*, *121*(5–6), 761–815. https://doi.org/10.1007/BF02590182

Koyanagi, R. Y., Tanigawa, W. R., & Nakata, J. S. (1988). Seismicity associated with the eruption. *The Puu Oo eruption of Kilauea Volcano, Hawaii: Episodes* (pp. 183–235).

Krumbholz, M., Hieronymus, C. F., Burchardt, S., Troll, V. R., Tanner, D. C., & Friese, N. (2014). Weibull-distributed dyke thickness reflects probabilistic character of host-rock strength. *Nature Communications*, *5*, 1–7. https://doi.org/10.1038/ncomms4272

Kwiatek, G., Plenkers, K., Nakatani, M., Yabe, Y., & Dresen, G., & JAGUARS-Group. (2010). Frequency-magnitude characteristics down to magnitude -4.4 for induced seismicity recorded at Mponeng Gold Mine, South Africa. *Bulletin of the Seismological Society of America*, *100*(3), 1165–1173. https://doi.org/10.1785/0120090277

Lahr, J. C., Chouet, B. A., Stephens, C. D., Power, J. A., & Page, R. A. (1994). Earthquake classification, location, and error analysis in a volcanic environment: Implications for the magmatic system of the 1989–1990 eruptions at Redoubt Volcano, Alaska. *Journal of Volcanology and Geothermal Research*, *62*(1–4), 137–151. https://doi.org/10.1016/0377-0273(94)90031-0

Latter, J. H. (1979). *Volcanological observations at Tongariro National Park. II: Types and classification of volcanic earthquakes, 1976-1978*. Report-Geophysics Division.

Latter, J. H. (1981). Volcanic earthquakes, and their relationship to eruptions at Ruapehu and Ngauruhoe volcanoes. *Journal of Volcanology and Geothermal Research*, *9*(4), 293–309. https://doi.org/10.1016/0377-0273(81)90041-x

Lazo, J., Basualto, D., Bengoa, C., Cardona, C., Franco, L., Gil-Cruz, F., et al. (2015). Spatial Distribution of b-value of the Copahue volcano during 2012-2014 eruptive period: Relationship between magmatic and hydrothermal system. *EGU general assembly conference abstracts*.

Lo Bascio, A., Luongo, G., & Nappi, G. (1973). Microtremors and volcanic explosions at Stromboli (Aeolian Islands). *Bulletin of Volcanology*, *37*(4), 596–606. https://doi.org/10.1007/bf02596894

Main, I. G. (1987). A characteristic earthquake model of the seismicity preceding the eruption of Mount St. Helens on 18 May 1980. *Physics of the Earth and Planetary Interiors*, *49*(3–4), 283–293. https://doi.org/10.1016/0031-9201(87)90030-6

Massin, F., Farrell, J., & Smith, R. B. (2013). Repeating earthquakes in the Yellowstone volcanic field: Implications for rupture dynamics, ground deformation, and migration in earthquake swarms. *Journal of Volcanology and Geothermal Research*, *257*, 159–173. https://doi.org/10.1016/j.jvolgeores.2013.03.022

McGarr, A. (2014). Maximum magnitude earthquakes induced by fluid injection. *Journal of Geophysical Research: Solid Earth*, *119*. https://doi.org/10.1002/2013JB010597

McGarr, A., & Barbour, A. J. (2018). Injection-induced moment release can also be aseismic. *Geophysical Research Letters*, *45*(11), 5344–5351. https://doi.org/10.1029/2018GL078422

McNutt, S. R. (1986). Observations and analysis of B-type earthquakes, explosions, and volcanic tremor at Pavlof Volcano, Alaska. *Bulletin of the Seismological Society of America*, *76*(1), 153–175.

McNutt, S. R. (2005). Volcanic Seismology. *Annual Review of Earth and Planetary Sciences*, *33*(1), 461–491. https://doi.org/10.1146/annurev.earth.33.092203.122459

McNutt, S. R., & Harlow, D. H. (1983). Seismicity at Fuego, Pacaya, Izalco, and San Cristobal Volcanoes, Central America, 1973–1974. *Bulletin of Volcanology*, *46*(3), 283–297. https://doi.org/10.1007/bf02597563

McNutt, S. R., & Roman, D. C. (2015). Volcanic seismicity. In *The encyclopedia of volcanoes* (pp. 1011–1034). Academic Press. https://doi.org/10.1016/b978-0-12-385938-9.00059-6

Miller, D., Foulger, G. R., & Julian, B. R. (1998). Non-double-couple earthquakes. 2. Observations. *Reviews of Geophysics*, *364*(98), 551–568. https://doi.org/10.1029/98rg00717

Minakami, T. (1960). Earthquakes and crustal deformation originating from volcanic activities. *Bulletin of the Earthquake Research Institute*, *38*, 497–544.

Minakami, T. (1974). Seismology of volcanoes in Japan. In *Developments in solid earth geophysics* (pp. 1–27). Elsevier. https://doi.org/10.1016/b978-0-444-41141-9.50007-3

Minakami, T., Hiraga, S., Miyazaki, T., & Utibori, S. (1969). Fundamental research for predicting volcanic eruptions. (Part 2). *Bulletin of the Earthquake Research Institute, University of Tokyo*, *47*(4–6), 42893.

Mogi, K. (1963). Magnitude-frequency relation for elastic shocks accompanying fractures of various materials and some related problems in earthquakes (2nd paper). *Bulletin of the Earthquake Research Institute, University of Tokyo*, *40*(4), 831–853.

Muirhead, J. D., Airoldi, G., White, J. D. L., & Rowland, J. V. (2014). Cracking the lid: Sill-fed dikes are the likely feeders of flood basalt eruptions. *Earth and Planetary Science Letters*, *406*, 187–197. https://doi.org/10.1016/j.epsl.2014.08.036

Muirhead, J. D., Van Eaton, A. R., Re, G., White, J. D. L., & Ort, M. H. (2016). Monogenetic volcanoes fed by interconnected dikes and sills in the Hopi Buttes volcanic field, Navajo Nation, USA. *Bulletin of Volcanology*, *78*(2), 1–16. https://doi.org/10.1007/s00445-016-1005-8

Murru, M., Montuori, C., Wyss, M., & Privitera, E. (1999). The locations of magma chambers at Mt. Etna, Italy, mapped by b-values. *Geophysical Research Letters*, *26*(16), 2553–2556. https://doi.org/10.1029/1999gl900568

Novelo-Casanova, D. A., Martinez-Bringas, A., & Valdés-González, C. (2006). Temporal variations of Qc− 1 and b-values associated to the December 2000–January 2001 volcanic activity at the Popocatepetl volcano, Mexico. *Journal of Volcanology and Geothermal Research*, *152*, 3347–4358. https://doi.org/10.1016/j.jvolgeores.2005.10.003

Odé, H. (1957). Mechanical analysis of the dike pattern of the Spanish Peaks area, Colorado. *The Geological Society of America Bulletin*, *68*, 567–576.

Park, I., Jolly, A., Kim, K. Y., & Kennedy, B. (2019). Temporal variations of repeating low frequency volcanic earthquakes at Ngauruhoe Volcano, New Zealand. *Journal of Volcanology and Geothermal Research*, *373*, 108–119. https://doi.org/10.1016/j.jvolgeores.2019.01.024

Peck, D. L., & Minakami, T. (1968). The formation of columnar joints in the upper part of Kilauean lava lakes, Hawaii. *The Geological Society of America Bulletin*, *79*(9), 1151–1166. https://doi.org/10.1130/0016-7606(1968)79[1151:tfocji]2.0.co;2

Petersen, T. (2007). Swarms of repeating long-period earthquakes at Shishaldin Volcano, Alaska, 2001–2004. *Journal of Volcanology and Geothermal Research*, *166*(3–4), 177–192. https://doi.org/10.1016/j.jvolgeores.2007.07.014

Power, J. A., Wyss, M., & Latchman, J. L. (1998). Spatial variations in the frequency-magnitude distribution of earthquakes at Soufriere Hills Volcano, Montserrat, West Indies. *Geophysical Research Letters*, *25*(19), 3653–3656. https://doi.org/10.1029/98gl00430

Ratchkovski, N. A., Wiemer, S., & Hansen, R. A. (2004). Seismotectonics of the central Denali fault, Alaska, and the 2002 Denali fault earthquake sequence. *Bulletin of the Seismological Society of America*, *94*. https://doi.org/10.1785/0120040621

Roberts, N. S., Bell, A. F., & Main, I. G. (2015). Are volcanic seismic b-values high, and if so when? *Journal of Volcanology and Geothermal Research*, *308*, 127–141. https://doi.org/10.1016/j.jvolgeores.2015.10.021

Ross, Z. E., Idini, B., Jia, Z., Stephenson, O. L., Zhong, M., Wang, X., et al. (2019). Hierarchical interlocked orthogonal faulting in the 2019 Ridgecrest earthquake sequence. *Science*, *366*(6463), 346–351. https://doi.org/10.1126/science.aaz0109

Rubin, A. M. (1995). Propagation of magma-filled cracks. *Annual Review of Earth and Planetary Sciences*, *23*, 287–336. https://doi.org/10.1146/annurev.ea.23.050195.001443

Rubin, A. M., Gillard, D., & Got, J.-L. (1998). A reinterpretation of seismicity associated with the January 1983 dike intrusion at Kilauea Volcano, Hawaii. *Journal of Geophysical Research*, *103*(5), 10003. https://doi.org/10.1029/97jb03513

Sánchez, J. J., McNutt, S. R., Power, J. A., & Wyss, M. (2004). Spatial variations in the frequency-magnitude distribution of earthquakes at Mount Pinatubo Volcano. *Bulletin of the Seismological Society of America*, *94*(2), 430–438.

Sandri, L., & Marzocchi, W. (2007). A technical note on the bias in the estimation of the b-value and its uncertainty through the least squares technique. *Annals of Geophysics*, *50*.

Saraò, A., Panza, G. F., Privitera, E., & Cocina, O. (2001). Non-double-couple mechanisms in the seismicity preceding the 1991-1993 Etna volcano eruption. *Geophysical Journal International*, *145*(2), 319–335. https://doi.org/10.1046/j.1365-246X.2001.01375.x

Scholz, C. H. (1968). The frequency-magnitude relation of microfracturing in rock and its relation to earthquakes. *Bulletin of the Seismological Society of America*, *58*(1), 399–415. https://doi.org/10.1785/bssa0580010399

Scholz, C. H. (2019). *The mechanics of earthquakes and faulting* (3rd ed., p. 493). Cambridge University Press.

Segall, P., Cervelli, P., Owen, S., Lisowski, M., & Miklius, A. (2001). Constraints on dike propagation from continuous GPS measurements. *Journal of Geophysical Research*, *106*(B9), 19301–19317. https://doi.org/10.1029/2001jb000229

Suzuki, S., & Kasahara, M. (1980). Seismic activity immediately before and in the early stage of the 1977 eruption of Usu Volcano, Hokkaido, Japan. *Journal of the Faculty of Science, Hokkaido University. Series 7, Geophysics*, *6*(1), 239–254.

Toda, S., Stein, R. S., Sagiya, T., & Turcotte, D. L. (2002). Evidence from the AD 2000 Izu islands earthquake swarm that stressing rate governs seismicity. *Nature*, *419*(6902), 58–61. https://doi.org/10.1038/nature00997

Tsukahara, H., & Ikeda, R. (1987). Hydraulic fracturing stress measurements and in-situ stress field in the Kanto—Tokai area, Japan. *Tectonophysics*, *135*(4), 329–345. https://doi.org/10.1016/0040-1951(87)90116-8

Tuffen, H., Dingwell, D. B., & Pinkerton, H. (2003). Repeated fracture and healing of silicic magma generate flow banding and earthquakes? *Geology*, *31*(12), 1089–1092. https://doi.org/10.1130/g19777.1

Turcotte, D. L. (1992). *Fractals and chaos in geology and geophysics*. Cambridge University Press.

Utsu, T. (1965). A method for determining the value of "b" in a formula log n= a-bm showing the magnitude-frequency relation for earthquakes. *Geophysical Bulletin of Hokkaido University*, *13*, 99–103.

Walker, G. P. L. (1986). Koolau Dike Complex, Oahu: Intensity and origin of a sheeted-dike complex high in a Hawaiian volcanic edifice. *Geology*, *14*(4), 310–313. https://doi.org/10.1130/0091-7613(1986)14<310:kdcoia>2.0.co;2

Walker, G. P. L. (1999). Volcanic rift zones and their intrusion swarms. *Journal of Volcanology and Geothermal Research*, *94*, 21. https://doi.org/10.1016/s0377-0273(99)00096-7

Walker, G. P. L., Eyre, P. R., Spengler, S. R., Knight, M. D., & Kennedy, K. (1995). Congruent dyke-widths in large basaltic volcanoes. In G. Baer, & A. Heimann (Eds.), *Physics and chemistry of dykes* (pp. 35–40). A. A. Balkema.

Warren, N. W., & Latham, G. V. (1970). An experimental study of thermally induced microfracturing and its relation to volcanic seismicity. *Journal of Geophysical Research*, *75*(23), 4455–4464. https://doi.org/10.1029/jb075i023p04455

Wiemer, S., & McNutt, S. R. (1997). Variations in the frequency-magnitude distribution with depth in two volcanic areas: Mount St. Helens, Washington, and Mt. Spurr, Alaska. *Geophysical Research Letters*, *24*(2), 189–192. https://doi.org/10.1029/96gl03779

Wiemer, S., McNutt, S. R., & Wyss, M. (1998). Temporal and three-dimensional spatial analyses of the frequency-magnitude distribution near Long Valley Caldera, California. *Geophysical Journal International*, *134*(2), 409–421. https://doi.org/10.1046/j.1365-246X.1998.00561.x

Wilks, M., Kendall, J. M., Nowacki, A., Biggs, J., Wookey, J., Birhanu, Y., et al. (2017). Seismicity associated with magmatism, faulting and hydrothermal circulation at Aluto Volcano, Main Ethiopian Rift. *Journal of Volcanology and Geothermal Research*, *340*, 52–67. https://doi.org/10.1016/j.jvolgeores.2017.04.003

Woods, J., Donaldson, C., White, R. S., Caudron, C., Brandsdóttir, B., Hudson, T. S., & Ágústsdóttir, T. (2018). Long-period seismicity reveals magma pathways above a laterally propagating dyke during the 2014–15 Bárðarbunga rifting event, Iceland. *Earth and Planetary Science Letters*, *490*, 216–229. https://doi.org/10.1016/j.epsl.2018.03.020

Wyss, M. (1973). Towards a physical understanding of the earthquake frequency distribution. *Geophys. Jour. Intl.*, *31*(4), 341–359. https://doi.org/10.1111/j.1365-246x.1973.tb06506.x

Wyss, M., Klein, F., Nagamine, K., & Wiemer, S. (2001). Anomalously high *b*-values in the South Flank of Kilauea volcano, Hawaii: Evidence for the distribution of magma below Kilauea's East rift zone. *Journal of Volcanology and Geothermal Research*, *106*(1–2), 23–37. https://doi.org/10.1016/s0377-0273(00)00263-8

Wyss, M., Shimazaki, K., & Wiemer, S. (1997). Mapping active magma chambers by *b* values beneath the off-Ito volcano, Japan. *Journal of Geophysical Research*, *102*(B9), 20413–20422. https://doi.org/10.1029/97jb01074

Yuan, A. T. E., McNutt, S. R., & Harlow, D. H. (1984). Seismicity and eruptive activity at Fuego volcano, Guatemala: February 1975–January 1977. *Journal of Volcanology and Geothermal Research*, *21*(3–4), 277–296. https://doi.org/10.1016/0377-0273(84)90026-x